Molecular Physics
Vol. 00, No. 00, Month 200x, 1–19

RESEARCH ARTICLE

Determination of interfacial tension of binary mixtures from perturbative approaches

F. J. Martínez-Ruiz[a,b] and F. J. Blas[a,b] *

[a] *Departamento de Física Aplicada, Facultad de Ciencias Experimentales, Universidad de Huelva, 21071 Huelva, Spain*

[b] *Centro de Investigación de Física Teórica y Matemática FIMAT, Universidad de Huelva, 21071 Huelva, Spain*

(*Received 00 Month 200x; final version received 00 Month 200x*)

We determine the interfacial properties of mixtures of spherical Lennard-Jones molecules from direct simulation of the vapor-liquid interface. We consider mixtures with the same molecular size but different dispersive energy parameter values. We use the extensions of the improved version of the inhomogeneous long-range corrections of Janeček [J. Janeček, *J. Phys. Chem. B* **129**, 6264 (2006)], presented recently by MacDowell and Blas [L. G. MacDowell and F. J. Blas, *J. Chem. Phys.* **131**, 074705 (2009)] and Martínez-Ruiz *et al.* [F. J. Martínez-Ruiz, F. J. Blas, B. Mendiboure, and A. I. Moreno-Ventas Bravo, *J. Chem. Phys.* **141**, 184701 (2014)], to deal with the interaction energy and microscopic components of the pressure tensor. We have performed Monte Carlo simulations in the canonical ensemble to obtain the interfacial properties of mixtures of Lennard-Jones molecules with a cutoff distances $r_c = 3\sigma$ in combination with the inhomogeneous long-range corrections. The pressure tensor is obtained using the mechanical (virial) and thermodynamic route. The vapour-liquid interfacial tension is also evaluated using three different procedures, the Irving-Kirkwood method, the difference between the macroscopic components of the pressure tensor, and the Test-Area methodology. This allows to check the validity of the recent extensions presented to deal with the contributions due to long-range corrections for intermolecular energy and pressure tensor in the case of binary mixtures. In addition to the pressure tensor and the surface tension, we also obtain density profiles, coexistence densities, and interfacial thickness as functions of pressure, at a given temperature. According to our results, the main effect of increasing the ratio between the dispersive energy parameters of the mixture, $\epsilon_{22}/\epsilon_{11}$, is to sharpen the vapour-liquid interface and to increase the width of the biphasic coexistence region. Particularly interesting is the presence of a relative maximum in the density profiles of the less volatile component at the interface. This maximum is related with adsorption or accumulation of these molecules at the interface, a direct consequence of stronger attractive interactions between these molecules in comparison with the rest of intermolecular interactions. In addition to that, the interfacial thickness decreases, the width of the tangential microscopic component of the pressure tensor profile increases, and the surface tension increases as $\epsilon_{22}/\epsilon_{11}$ is larger.

Keywords: Interfacial tension, interfacial properties, binary mixtures of Lennard-Jones, Monte Carlo simulation, Test-Area, Volume Perturbation, Irving-Kirkwood, microscopic components of pressure tensor, macroscopic components of pressure tensor.

1. Introduction

Fluid-fluid interfaces have fascinated scientifics since the time of Laplace and Young [1]. More recently, interfacial properties, and particularly interfacial tension, have been routinely determined for many computer simulation researchers of the liquid-state community. However, the application of theories of inhomogeneous systems,

*Corresponding author. Email: felipe@uhu.es

ISSN: 0040-5167 print/ISSN 1754-2278 online

DOI: 10.1080/0040516YYxxxxxxxx
http://www.informaworld.com

and especially computer simulation, to fluids mixtures is far less common. Knowledge of interfacial properties of mixtures is essential in a large number of scientific and engineering fields, including nucleation or dynamics of phase transition, among many others. From a formal point of view, understanding how miscroscopic parameters (for instance, molecular size and dispersive energy interactions) determine the thermodynamic and structural behaviour of mixtures near interfaces is one of the classical problems in applied Statistical Mechanics and computer simulation.

Surface tension is probably the most challenging property to be determined and predicting using molecular-based theories and simulation techniques. Despite the number of studies carried out since computer simulation is used routinely for determining the properties of a molecular model, the calculation of surface tension is still a subtle problem. The ambiguity in the definition of the microscopic components of the pressure tensor [2, 3], the finite size effects due to capillary waves [4, 5], or the difficulty for the calculation of the dispersive long-range corrections (LRC) associated to the intermolecular interactions [6, 7], make the calculation of surface tension a difficult and non-trivial problem.

The usual procedure to the evaluation of the fluid-fluid interfacial tension in a molecular simulation involves the determination of the microscopic components of the pressure tensor through the well-known mechanical or virial route. This route states that surface tension of a planar fluid-fluid interface can be readily obtained from the integration of the difference between the normal and tangential microscopic components of the pressure tensor profiles along the interface. This method generally involves an ensemble average of the virial of Clausius according to the recipes of Irving and Kirkwood [8]. Although the mechanical route is an appropriate technique for determining the surface tension, a number of alternative methods have been proposed during the last years to calculate, not only the interfacial tension, but also for the components of the pressure tensor, without the need of evaluate the virial.

These new methods can be viewed as a collection of effective and elegant techniques based on the thermodynamic definition of surface tension and tensore pressure. The first one can be understood as the change in free energy when the interfacial area is changed, at constant volumen and temperature. The second one, can be expressed as the change in free energy when the volume of the system is changed along any direction, keeping constant the other two dimensions. Examples of these methods are the Test-Area (TA) technique of Gloor *et al.* [3], the Volume Perturbation (VP) method of de Miguel and Jackson [9–11], the Wandering Interface Method (WIM), introduced by MacDowell and Bryk [12], and the use of the Expanded Ensemble (EE), based on the original work of Lyuvartsev *et al.* [13], for calculating the surface tension proposed independently by Errington and Kofke [14] and de Miguel [15]. These methods are becoming very popular and are being used routinely to determine the vapour-liquid interfacial properties of different potential model fluids [7, 16–35].

As mentioned previously, one of the major difficulties encountered in the simulation of inhomogeneous systems by molecular simulation is the truncation of the intermolecular potential. Although for homogeneous systems this issue is easily solved by including the well-known homogeneous LRC [36, 37], the situation is much more complicated in the case of fluid-fluid interfaces, and in general, in inhomogeneous systems. Fortunately, this problem seems to solved satisfactorily recently in cases in which the system exhibits planar symmetry. Different authors have contributed to the establishment of appropriate and standard inhomogeneous LRC, including Blokhius [38], Mecke [39, 40], Daoulas [41], Guo and Lu [42], and finally, Janeček [6, 43], and the recent improved methods proposed by MacDowell

and Blas [7], de Gregorio *et al.* [33], and Martínez-Ruiz *et al.* [34]

The goal of this work is to determine the vapor-liquid interfacial properties of mixtures of spherical LJ molecules with the same molecular size but different dispersive energy parameters. In particular, we focus on the effect of the dispersive energy ratio on different interfacial properties, including density profiles, normal and tangential microscopic components of the pressure tensor profiles, and surface tension. In addition to that, we also analyze the effect of the dispersive energy ratio on other thermodynamics properties, such as coexistence density and pressure-composition slices of the phase diagram. In all cases, we use the improved versions of the inhomogenenous LRC of Janeček [6] recently proposed by MacDowell and Blas [7] for the intermolecular energy and Martínez-Ruiz *et al.* [34] for the microscopic components of the pressure tensor. In order to check the effectiveness of these methods in the case of mixtures, we also determine the surface tension and the components of the pressure tensor using two different perturbative methods, the TA technique and the VP methodology. This allows to obtain independent results and compare our predictions with simulation data taken from the literature. To our knowledge, this is the first time the surface tension and components of the pressure tensor of mixtures of LJ spheres are calculated using perturbative methods in both cases and taking into account the LRC associated to the intermocular potential and components of the pressure tensor.

The rest of the paper is organized as follows. In Section II we present the model and simulation details of this work. Results obtained are discussed in Section III. Finally, in Section IV we present the main conclusions.

2. Model and simulation details

We consider binary mixtures of spherical LJ molecules characterized by diameters σ_{ii} and dispersive energies ϵ_{ii}, where index i denotes component i. The interaction potential between two different molecules of species i and j is given by,

$$u_{ij}^{LJ}(r) = 4\epsilon_{ij}\left[\left(\frac{\sigma_{ij}}{r}\right)^{12} - \left(\frac{\sigma_{ij}}{r}\right)^{6}\right] \tag{1}$$

where r is the distance between two molecules, and σ_{ij} and ϵ_{ij} are the intermolecular parameters (size and dispersive energy) associated to the interaction between molecules of type i and j. In this work, we use the well-known Lorentz-Berthelot combining rules for unlike dispersive interactions,

$$\sigma_{ij} = \frac{\sigma_{ii} + \sigma_{jj}}{2} \tag{2}$$

and

$$\epsilon_{ij} = (\epsilon_{ii}\epsilon_{jj})^{1/2} \tag{3}$$

During the simulation, we use a potential spherically truncated (but not shifted) at a cutoff distance r_c, defined by,

$$u_{ij}(r) = u_{ij}^{LJ}(r)\ [1 - \Theta(r - r_c)] = \begin{cases} u_{ij}^{LJ}(r) & r \leq r_c \\ 0 & r > r_c \end{cases} , \tag{4}$$

where $\Theta(x)$ is the Heaviside step function. Note that since we restrict our study to binary mixtures with the same size, $\sigma_{11} = \sigma_{22} = \sigma_{12}$, we also use the same cutoff distance r_c for all the interactions.

We examine mixtures interacting with this spherically truncated potential model with cutoff distance $r_c = 3\sigma$ and several interaction dispersive parameter values $\epsilon_{22}/\epsilon_{11}$. Standard homogeneous LRC to the intermolecular interaction energy and pressure [37] are used in NPT simulations of bulk phases. In addition to that, inhomogeneous LRC using the MacDowell and Blas [7, 44] methodology for the intermolecular potential energy and the recipe presented in our recent paper [34], based on the Janeček's method [6, 43], for the evaluation of the LRC for the components of the pressure tensor. Results obtained using these LRC are equivalent to use the full potential or a potential with infinite truncation distance.

The number of molecules, N, used in the simulations performed in this work for studying the vapour-liquid interface of mixtures of LJ molecules varied from $N = 2150$, for the lowest pressure considered ($P^* = P\sigma_{11}^3/\epsilon_{11} = 0.06$), to $N = 2750$, for the highest pressure analyzed ($P^* = P\sigma_{11}^3/\epsilon_{11} = 0.16$). Note that it is not possible to have systems with the same total number of molecules and with the same interfacial area since we are dealing with binary mixtures in which composition must be taken into account. Whereas the initial setup for simulations of vapour-liquid interfaces for pure systems is relatively easy, the initial configuration of a vapour-liquid interface involving binary mixtures is a delicate issue. To obtain the initial interfacial simulations boxes at different pressures, we firstly use the well-known Soft-SAFT approach, based on Wertheim's Thermodynamic Perturbation Theory [45–48], and developed by one of us [49, 50], to calculate the complete phase diagrams of the mixtures to be studied. This allows to have an initial precise picture of the coexistence envelope of the system at thermodynamic conditions at which the simulations are performed. In particular, initial densities and compositions of each component of the mixture in both, the vapour and liquid phases, are obtained using the Soft-SAFT approach for the mixtures considered in this work.

Simulations are performed in two steps. In the first step, homogeneous liquid and vapour systems, at a given temperature and pressure, are equilibrated in a rectangular simulation box of dimensions $L_x = L_y = 10\sigma$, and varying L_z. Box length measured along the z-axis is chosen in such a way that the corresponding densities match the predictions obtained from the Soft-SAFT approach at temperature and pressure selected. In addition to that, the particular number of molecules of each species, in both liquid and vapour phases, are also selected according to the SAFT predictions. Both simulation boxes (liquid and vapour phases) are equilibrated at the same temperature and pressure using an NPT ensemble in which L_x and L_y are kept constant and only L_z is varied along the simulation. NPT simulations of homogeneous phases are organized by cycles. A cycle is definied as N trial moves (displacement of the center of mass) and an attempt to change the box length along the z-axis (L_z). The magnitude of the appropriate displacement is adjusted so as to get an acceptance rate of 30 % approximately. We use periodic boundary conditions and minimum image convention in all three directions of the simulation box. In addition to that, homogeneous LRC corrections to the intermolecular energy and pressure are also used [37].

In a second step, the interfacial simulation box is prepared leaving the previous

homogeneous liquid phase at the center of the new box with the same homogeneous vapour phase boxes of equal size previously prepared at each side. Since L_x and L_y ($\mathcal{A} = L_x L_y$, i.e., the interfacial area) is the same for all homogeneous phases, it is always posible to build up the interfacial simulation box as explained here. The final overall dimensions of the vapour-liquid-vapour simulation box are therefore $L_x = L_y = 10\sigma$, and $L_z = 78.17\sigma$ for the lowest pressure considered ($P^* = k_B T/\epsilon = 0.70$), and $L_z = 99.48\sigma$ for the highest pressure ($P^* = k_B T/\epsilon = 1.1$).

The simulations for studying the vapour-liquid interface are also organized in cycles. In this case, a cycle is defined as N trial moves (displacement of the center of mass) and the magnitude of the appropriate displacement is adjusted so as to get an acceptance rate of 30 % approximately. We use periodic boundary conditions and minimum image convention in all three directions of the simulation box. To be consistent with simulations performed using the NPT ensemble for preparing the definitive simulation box, we use inhomogeneous LRC to the intermolecular energy of MacDowell and Blas [7, 44] methodology for the intermolecular potential energy and the recipe presented in our previous paper [34] for the evaluation of the LRC for the components of the pressure tensor, both of them based on the Janeček's method [6].

We have obtained the normal and tangential microscopic components of the pressure tensor from the mechanical expression or virial route,

$$P_{\alpha\beta} = \left\langle \rho k_B T \right\rangle + \left\langle \frac{1}{V} \sum_{i=1}^{N-1} \sum_{j=i+1}^{N} r_{ij}^{\alpha} f_{ij}^{\beta} \right\rangle \tag{5}$$

In this work, we have followed the same procedure as in our previous work [34] and used the well-known Irving and Kirkwood (IK) recipe [8, 51] for determining the microscopic components of the pressure tensor, $P_N(z) \equiv P_{zz}(z)$ and $P_T(z) \equiv P_{xx}(z) \equiv P_{yy}(z) \equiv \frac{1}{2}(P_{xx}(z) + P_{yy}(z))$. The components of the pressure tensor are calculated each cycle.

Following de Miguel and Jackson [9], we have also determined the macroscopic components of the pressure tensor using its thermodynamic defintion as,

$$P_{\alpha\alpha} = -\left(\frac{\partial F}{\partial V}\right)_{NTL_{\beta\neq\alpha}} \tag{6}$$

The notation $L_{\beta\neq\alpha}$ indicates that the partial derivative with respect to the volume is performed in such a way that the dimension of the system along the α-axis, L_α, is varied while keeping all other dimensions L_β ($\beta \neq \alpha$) fixed.

We follow the methodology proposed by de Miguel and Jackson [9], based on the seminal works of Eppenga and Frenkel [52] and Harismiadis *et al.* [53], an use virtual volume perturbations of magnitude $\xi = \Delta V/V$ every five MC cycles. Here ξ defines the relative volume (compressive and expansive) change associated with the perturbation, i.e., rescale independently the box lengths of the simulation cell and positions of the molecular centers of mass according to linear transformations along the appropriate directions. In all cases, eight different (positive and negative) relative volume changes in the range $2 \times 10^{-4} \leq |\xi| \leq 15 \times 10^{-4}$ are used in our calculations. The final values of the macroscopic components of the pressure tensors presented in this work, P_N and P_T, correspond to the extrapolated values (as determined by a linear extrapolation to $|\xi| \to 0$ of the values obtained from

increasing-volume and decreasing-volume perturbations) obtained from a combined compression-expansion perturbation.

Surface tension is determined using three independent routes. In the first one, we used the mechanical definition that involves the integration of the difference between the tangential and normal microscopic components of the pressure tensor profiles, as obtained from the IK methodology, along the simulation box according to,

$$\gamma = \int_0^{L_z} \left(P_N(z) - P_T(z)\right)\, dz \tag{7}$$

Note that here we have chosen the z-axis perpendicular to the interface and the integral is performed along the total length L_z of the simulation box.

In the second route,the surface tension is calculated using the thermodynamic definitions of P_N and P_T, as proposed by de Miguel and Jackson [9]. The surface tension is obtained as,

$$\gamma = L_Z(P_N - P_T) \tag{8}$$

Here L_z is the simulation length along the z-axis. Note that Eq. (8) can be viewed as the macroscopic version of Eq. (7). As in the case of the microscopic definition, since there exist two vapour-liquid interfaces, the true value associated to a single interface is half of the value obtained from Eqs. (7) and (8).

Finally, in the third route we use TA methodology [3], which is based in the thermodynamic definiton of surface tension as,

$$\gamma = \left(\frac{\partial F}{\partial \mathcal{A}}\right)_{NVT} \tag{9}$$

Since the method is a standard and well-known procedure for evaluating fluid-fluid interfacial tensions of molecular systems, here we only provide the most important features of the technique. For further details we recommend the original work [3] and the most important applications [7, 9, 16, 19–24, 27, 28, 33, 44, 54–57]. The implementation of the TA technique involves performing virtual or test area deformations of relative area changes defined as $\xi = \Delta\mathcal{A}/\mathcal{A}$ during the course of the simulation at constant N, V, and T every five MC cycles. As shown by Gloor *et al.* [3], the surface tension follows from the computation of the change in Helmholtz free energy associated with the perturbation, which in turn can be expressed as an ensemble average of the corresponding Boltzmann factor. Further details can be found in Ref. [3] Note that the procedure for calculating the surface tension is similar to that used to evaluate the components of the pressure tensor, but in this case the changes in the normal and transverse dimensions are coupled to keep the overall volume constant. In particular, we use the same number and values for the relative area changes ξ, and the same procedure to obtain the extrapolated values.

We typically consider six reduced pressures in the range $P^* = P\sigma_{11}^3/\epsilon_{11} = 0.06$ up to 0.16. In the case of NPT simulations of the homogeneous liquid and vapour phases prepared in the first step, each simulation box is equilibrated for 10^6 MC cycles. In the case of the NVT simulations corresponding to the interfacial box, the system is also well equilibrated for other 10^6 equilibration MC cycles. In addition to that, averages are determined over a further period of 2×10^6 MC cycles. The

production stage is divided into M blocks. Normally, each block is equal to 10^5 MC cycles. The ensemble average of the macroscopic components of the pressure tensor and the surface tension is given by the arithmetic mean of the block averages and the statistical precision of the sample average is estimated from the standard deviation in the ensemble average from $\overline{\sigma}/\sqrt{M}$, where $\overline{\sigma}$ is the variance of the block averages, and $M = 20$ in all cases.

All the quantities in our paper are expressed in conventional reduced units of component 1, with σ_{11} and ϵ_{11} being the length and energy scaling units, respectively. Thus, the temperature is given in units of ϵ_{11}/k_B, the densities of both components and the total density in units of σ_{11}^{-3}, the bulk pressure and components of the pressure tensor in units of the $\epsilon_{11}/\sigma_{11}^3$, the surface tension in units of $\epsilon_{11}/\sigma_{11}^2$, and the cutoff distance and interfacial thickness in units of σ_{11}.

3. Results and discussion

In this section we present the main results from simulations of the vapour-liquid interface of mixtures of spherical LJ molecules using LRC for the intermolecular potential energy and components of the pressure tensor. We focus mainly on the effect of the dispersive energy interaction between the components of the mixture on several interfacial properties. We have determined the components of the pressure using both the mechanical (or virial) and thermodynamic routes. Comparison between both results allows to check the validity of the method presented in previous works [7, 34, 44] for determining the contribution to the energy and pressure due to the LRC in mixtures of LJ systems. We have also examined several coexistence properties, such as coexistence densities, and also other interfacial properties, including density profiles, interfacial thickness, and surface tension. As in our previous work for pure systems [34], we pay special attention on the determination of the the vapour-liquid interfacial tension calculated using different routes, including the mechanical or virial route (using the traditional IK methodology) and the thermodynamic definition (using the VP and TA methods) of the surface tension.

We first analyze the effect of the dispersive energy parameter between components of the mixtures on density profiles. We follow the same analysis and methodology than in our previous works [7, 16, 34, 44, 54, 56] and consider different dispersive energy parameters and pressures. The equilibrium density profiles of each of components of the mixture, $\rho_1(z)$ and $\rho_2(z)$, as well as the total density, $\rho(z) = \rho_1(z) + \rho_2(z)$, are computed from averages of the histogram of densities along the z direction over the production stage. The bulk vapour and liquid densities of both components and the total density are obtained by averaging $\rho_1(z)$, $\rho_2(z)$, and $\rho(z)$, respectively over appropriate regions sufficiently removed from the interfacial region. This procedure is meaningful as far as the central liquid slab is thick enough. This turns out to be the case in our simulations, including those performed at the higher pressure. The bulk vapour densities are obtained after averaging the corresponding density profiles on both sides of the liquid film. The statistical uncertainty of these values is estimated from the standard deviation of the mean values. Following our previous works, additional interfacial properties, such as the position of the Gibbs-dividing surface, z_0, and the $10 - 90$ interfacial thickness, t, are obtained by fitting each of the equilibrium density profiles to hyperbolic tangent functions [1] (see Eq. (3) of our previous work [16] for further details). We fix liquid, ρ_L, and vapour, ρ_V, densities for each component and for the total density to previously computed values and treat z_0 and t as adjustable parameters.

Our simulation results for the bulk densities of each component, total densities, molar fractions of both component in each, components of the pressure tensor, surface tension, and interfacial thickness for mixtures of LJ molecules interacting with different dispersive energy parameters and the full potential, at different pressures, are collected in Tables 1 and 2.

We show in Fig. 1 the density profiles $\rho_1(z)$, $\rho_2(z)$, and $\rho(z)$ for three mixtures of LJ molecules with the same size, $\sigma_{22} = \sigma_{11}$ and different dispersive energy parameters of the component 2, $\epsilon_{22}/\epsilon_{11} = 1.50$, 1.75, and 2.00, at $T = 1.6$ and several pressures. For the sake of clarity, we only present one half of the profiles corresponding to one of the interfaces. Also for convenience, all density profiles have been shifted along z so as to place z_0 at the origin. As can be seen, for a given mixture (or value of the dispersive energy parameter $\epsilon_{22}/\epsilon_{11}$), the slope (in absolute value) of the density profiles corresponding to component 1 and total density in the interfacial region decreases as the pressure is increased, making smaller the jump in densities when passing from the vapour to the liquid side of the interface. Consequently, the interfacial thickness increases, an expected behaviour that indicates the phase envelope is becoming thicker as the system approaches to the critical point of the mixture.

Fig. 1 also shows the effect of increasing the dispersive energy parameter $\epsilon_{22}/\epsilon_{11}$ on the density profiles, i.e., when the mixture becomes more asymmetric. As can be seen comparing parts (a), (b), and (c) of the figure, an increase of $\epsilon_{22}/\epsilon_{11}$ results in steeper density profiles of component 1 and total density along the interfacial region. This effect, which also produces narrower interfacial regions, is related with the increasing of the asymmetry of the mixture. As $\epsilon_{22}/\epsilon_{11}$ becomes larger, the mixture is more asymmetric and the phase envelope (see Fig. 2) becomes wider in terms of densities (and also in molar fractions), or in other words, jumps in density from the vapour to the liquid side of the interface increases.

Special attention deserves the behaviour of the density profiles corresponding to the component 2 of the system, the less volatile substance of the mixture. As can be seen inf Fig. 1, $\rho_2(z)$ exhibits a nearly monotonic increasing behaviour when passing from the vapour to the liquid size of the interface when $\epsilon_{22}/\epsilon_{11} = 1.50$. However, as the difference in dispersive energies between both components increases, $\epsilon_{22}/\epsilon_{11} = 1.75$ and 2.00, $\rho_2(z)$ exhibits a relative maximum at the interface. This maximum is related with adsorption of component 2 at the interface. These molecules tend to accumulate at the interface on increasing the dispersive energy parameter of component 2 and decreasing of the pressure. This type of enhanced adsorption of one component relative to the other is usually seen in binary mixtures of spherical molecules when there are significant differences in the values of the unlike dispersion interactions [58].

The vapour-liquid phase envelopes of mixtures of LJ molecules with different dispersion interaction values $\epsilon_{22}/\epsilon_{11}$, as calculated from the analysis of the density profiles obtained from our Monte Carlo simulations, are depicted in Fig. 2. The Soft-SAFT theoretical approach has been also used to obtain the complete phase diagram of mixtures of LJ molecules with different dispersive interation parameter values. Although, as we have mentioned in the Introduction and Model and simulation details sections, we have used the information from the theory for obtaining initial guesses of the liquid and vapour densities and compositions of mixtures to be studied by simulation at particular thermodynamic conditions, this theoretical predictions can also be used as results to compare our simulation results and check the ability of SAFT in predicting the phase behaviour of these mixtures. As can be seen in part (a) of the figure, the pressure-density or $P\rho$ slice of the phase diagram of mixture indicates that the phase envelope of the system, at $T = 1.60$, becomes

wider as the dispersive energy parameter $\epsilon_{22}/\epsilon_{11}$ is increased. The enlargement of the width associated to the phase envelope is essentially due to the increase of the liquid density as the dispersive energy is higher. As can be seen, agreement between Monte Carlo simulation results and prediction from SAFT is excellent in all cases. It is important to recall here that results from the theory are predictions obtained using the Lorentz-Berthelot combining rules without any further fitting procedure. We have also obtained the pressure-composition or Px slice of the mixture at the same thermodynamic conditions and using the same dispersive energy parameters. As can be seen in part (b) of the figure, we have presented the molar fractions of the three mixtures from the analysis of the density profiles, as well as the predictions obtained from the Soft-SAFT. The phase diagrams show the expected behaviour, in agreement with part (a) of the figure: as the asymmetry of the system is increased (higher values of $\epsilon_{22}/\epsilon_{11}$), the phase envelope of the mixture also increases. As can be seen, the region at which the system exhibits vapour-liquid phase separation increases in compositions and pressures, an expected behaviour of mixtures that exhibit type I phase behaviour according to the classification of Scott and Konynenburg [59, 60]. Agreemenet between Monte Carlo simulation and theoretical predictions is excellent in all cases. In summary, increasing the dispersive energy parameter $\epsilon_{22}/\epsilon_{11}$ results in larger cohesive energy in the system, which manifiests as wider phase envelopes and larger critical pressures.

Once we have studied the phase equilibria properties of the mixtures studied form the analysis of the density profiles, we now turn on the study of other interfacial properties of mixtures of LJ systems with different dispersion interactions. We analyze the equilibrium normal and tangential components of the microscopic pressure tensor profiles, $P_N(z)$ and $P_T(z)$, respectively, of mixtures of LJ molecules with different dispersive energy parameters. The profiles are computed from averages of histograms of pressures along the z direction over the production stage, according to the IK prescription explained in Section II. As we have mentioned previously, this procedure is meaningful as far as the central liquid slab is thick enough. In addition to the methododology of IK, based on the mechanical route, we have also determined the macroscopic components of the pressure tensor. In particular, we have averaged the normal microscopic component of the pressure tensor obtained from the IK along the vapour phase (P_N^{vir}). We have also calculated the normal and tangential components of the pressure tensor from the thermodynamic route (P_N and P_T). It is important to recall here that all calculations presented in this work are obtained using LRC for the intermolecular energy and pressure following the improved method proposed previously by MacDowell and Blas and Martínez-Ruiz *et al.*, based on the Janeček's methodology [6], as explained in Section II. This means that both routes, mechanical and thermodynamic, take into account explicitly the LRC. Results from the different routes are presented in Table 2. As can seen, agreement between all results is excellent in all cases.

We consider the normal and tangential components of the microscopic pressure tensor profiles at $T = 1.6$ and several pressures. As can be seen in Fig. 3, the components of the microscopic pressure tensor along the two vapour-liquid interfaces exhibit the expected behaviour, i.e., the normal component of the pressure tensor profile is constant (within the expected statistical error) through the interface and equal to the vapour pressure of the system (according to the mechanical stability, that it requires the gradient of pressure tensor vanishes). In addition, the tangential component of the pressure tensor profile is approximately constant and equal to the normal pressure in the liquid and both vapour bulk-like regions of the simulation box. $P_T(z)$ becomes negative at the two interfacial regions of the system showing two (negative) local minima. As can be seen, negative contributions to the tangen-

tial pressure became more negative as the dispersive energy parameter $\epsilon_{22}/\epsilon_{11}$ is increased. This produces more tension along the interface, decreasing the interfacial thickness of the system (as previously shown in the density profiles of Fig. 1). As we will see later, this produces higher interfacial tension, in agreement with the results already presented. An interesting feature observed in the pressure profiles, also seen in pure systems [34], is that there are regions at which $P_T(z) < P_N(z)$, located at the vapour-liquid interface, corresponding to zones of tension. Contrary, small locations at the interface corresponding to zones near the vapour bulk-like regions, are regions of compression in which $P_T(z) > P_N(z)$. The reason for which the transverse pressure has values greater than P_N at the interface near the vapour phase and large negative values (and lower than P_N) at other locations of the interface is a consequence of the behaviour of the pressure in the unstable bulk phase region (spinodal region), which plays an essential role in the physics at interfaces. For further details we recommend the excellent review of Davies and Scriven [61].

Another interesting property obtained from our analysis is the $10-90$ interfacial thickness (cf. Table 2). For a given cutoff distance, t is seen to increase with pressure, which simply reflects the fact that the interfacial region gets correspondingly thinner, in agreement with our previous results. This behaviour may be clearly seen in Fig. 4. At low pressure the density profiles exhibit a sharp interface, which corresponds to a low value of the interfacial thickness. As the pressure is increased towards the critical value, the interfacial region becomes wider, and hence, the value of the interfacial thickness increases. The variation of interfacial thickness with the dispersive energy parameter $\epsilon_{22}/\epsilon_{11}$ can be seen in the same figure. As can be seen, an increase of $\epsilon_{22}/\epsilon_{11}$, at constant pressure, results in a decreased of the interfacial thickness, which is consistent with the fact that the systems with larger dispersive energies have a larger cohesive energy. This behaviour is also consistent with that found for the shape of the vapour-liquid phase envelopes.

Finally, we have calculated the vapour-liquid interfacial tension of mixtures of LJ molecules using several dispersive energy parameters $\epsilon_{22}/\epsilon_{11}$. In particular, we have determined the surface tension using its mechanical definition that involves the integration of the difference between the tangential and normal microscopic components of the pressure tensor profiles, as obtained from the IK methodology, along the simulation box according to Eq. (7). In addition to that, we have also determined the surface tension using two perturbative approaches: the Test-Area (TA) method of Gloor *et al.* [3] and the VP technique of de Miguel and Jackson [9]. In first case, the surface tension is determined performing virtual area perturbations of a (small) magnitude during the course of the simulation at constant volume. In the second case, the surface tension is determined in two steps. In the first step, the normal and tangential macroscopic components of the pressure tensor, P_N and P_T, are calculated from their thermodynamic definitions as proposed by de Miguel and Jackson [9]. In the second step, the surface tension γ is obtained from Eq. (8) (see Eq. (21) of the work of de Miguel and Jackson [9]).

The calculation of the surface tension through three different but complementary routes allows to compare the results obtained from the mechanical and thermodynamic methods. This is another convincing test for consistency for the inhomogeneous LRC presented in our previous works for mixtures. Note that similar consistent results have been found in previous applications of the method for calculating the total potential energy of the system [7, 44, 54, 56].

The pressure dependence of the interfacial tension for mixtures of LJ molecules interacting with different dispersive energy parameters $\epsilon_{22}/\epsilon_{11}$ is shown in Fig. 5. Agreement between our independent simulations demonstrates that both methodologies are fully equivalent for all the systems and conditions studied. As can be

seen, at any given pressure, the interfacial tension is larger for molecules with larger values of $\epsilon_{22}/\epsilon_{11}$. Once again, this is consistent with the larger cohesive energy in systems consisting of molecules in which attractive interactions are longer.

4. Conclusions

We have simulated the interfacial properties of the vapor-liquid interface of mixtures of spherical LJ molecules. Three mixtures of molecules with the same molecular size but different dispersive energy parameters are considered. The intermolecular interactions are truncated at a cutoff distance of 3σ, σ being the diameter of the molecules, and inhomogeneous long-range corrections for dispersive interactions and pressure tensor are used. The microscopic and macroscopic components of normal and tangential pressure are determined using two different routes, their mechanical (virial route) and thermodynamic (virtual pressure route) definitions. The interfacial tension is also evaluated using three different procedures, the Irving-Kirkwood method, the difference between the macroscopic components of the pressure tensor, and the Test-Area methodology. We have examined the density profiles, interacial thickness, and surface tension in terms of the pressure and the dispersive energy paremeter ratio $\epsilon_{22}/\epsilon_{11}$. In addition, we have also calculated the coexistence diagram (pressure *versus* density) and the pressure-composition slice of the phase diagram at a constant temperature from an analysis of the density profiles.

The effect of the dispersive energy parameters of the mixture, $\epsilon_{22}/\epsilon_{11}$, on density profiles, microscopic components of the normal and tangential pressure tensor profiles, coexistence densities, interfacial thickness, and interfacial tension has been investigated. The vapor-liquid interface is seen to sharpen with increasing dispersive energy ratio corresponding to an increase in the width of the coexistence phase envelope and the pressure-composition slice of the phase diagram and an accompanying increase in the surface tension.

Acknowledgments

The authors would like to acknowledge helpful discussions with A. I. Moreno-Ventas Bravo. This work was supported by Ministerio de Ciencia e Innovación through Grant with reference FIS2010-14866 and Ministerio de Economía y Competitividad through Grant with reference FIS2013-46920-C2-1-P. Further financial support from Junta de Andalucía and Universidad de Huelva is also acknowledged.

References

[1] J. S. Rowlinson and B. Widom, *Molecular Theory of Capillarity* (Claredon Press, 1982).
[2] F. Varnik, J. Baschnagel, and K. Binder, J. Chem. Phys. **113**, 4444 (2000).
[3] G. J. Gloor, G. Jackson, F. J. Blas, and E. de Miguel, J. Chem. Phys. **123**, 134703 (2005).
[4] L. G. MacDowell, J. Benet, and N. A. Katcho, Phys. Rev. Lett. **111**, 047802 (2013).
[5] L. G. MacDowell, J. Benet, N. A. Katcho, and J. M. Palanco, Adv. Colloid Interface Sci. **206**, 150 (2014).
[6] J. Janeček, J. Phys. Chem. B **110**, 6264 (2006).
[7] L. G. MacDowell and F. J. Blas, J. Chem. Phys. **131**, 074705 (2009).
[8] J. H. Irving and J. G. Kirkwood, J. Chem. Phys. **18**, 817 (1950).
[9] E. de Miguel and G. Jackson, J. Chem. Phys. **125**, 164109 (2006).
[10] E. de Miguel and G. Jackson, Mol. Phys. **104**, 3717 (2006).
[11] P. E. Brumby, A. J. Haslam, E. de Miguel, and G. Jackson, Mol. Phys. **109**, 169 (2010).
[12] L. G. MacDowell and P. Bryk, Phys. Rev. E **75**, 061609 (2007).
[13] A. P. Lyuvartsev, A. A. Martsinovski, S. V. Shevkunov, and P. N. Vorontsov-Velyaminov, J. Chem. Phys. **96**, 1776 (1992).

[14] J. R. Errington and D. A. Kofke, J. Chem. Phys. **127**, 174709 (2007).
[15] E. de Miguel, J. Phys. Chem. B **112**, 4647 (2008).
[16] F. J. Blas, L. G. MacDowell, E. de Miguel, and G. Jackson, J. Chem. Phys. **129**, 144703 (2008).
[17] G. Galliero, J. Chem. Phys. **133**, 074705 (2010).
[18] A. Ghoufi and P. Malfreyt, Mol. Simul. **39**, 603 (2013).
[19] C. Vega and E. de Miguel, J. Chem. Phys. **126**, 154707 (2007).
[20] J. M. Míguez, D. González-Salgado, J. L. Legido, and M. M. Piñeiro, J. Chem. Phys. **132**, 184102 (2010).
[21] G. Galliero, M. M. Piñeiro, B. Mendiboure, C. Miqueu, T. Lafitte, and D. Bessières, J. Chem. Phys. **130**, 104704 (2009).
[22] E. de Miguel, N. G. Almarza, and G. Jackson, J. Chem. Phys. **127**, 034707 (2007).
[23] C. Miqueu, J. M. Míguez, M. M. Piñeiro, T. Lafitte, and B. Mendiboure, J. Phys. Chem. B **115**, 9618 (2011).
[24] F. Biscay, A. Ghoufi, V. Lachet, and P. Malfreyt, J. Chem. Phys. **131**, 124707 (2009).
[25] A. Ghoufi, F. Goujon, V. Lachet, and P. Malfreyt, J. Chem. Phys. **128**, 154716 (2008).
[26] A. Ghoufi, F. Goujon, V. Lachet, and P. Malfreyt, Phys. Rev. E **77**, 031601 (2008).
[27] F. Biscay, A. Ghoufi, F. Goujon, and P. Malfreyt, J. Phys. Chem. B **112**, 13885 (2008).
[28] F. Biscay, A. Ghoufi, F. Goujon, V. Lachet, and P. Malfreyt, J. Chem. Phys. **130**, 184710 (2009).
[29] F. Biscay, A. Ghoufi, V. Lachet, and P. Malfreyt, Phys. Chem. Chem. Phys. **11**, 6132 (2009).
[30] J. C. Neyt, A. Wender, V. Lachet, A. Ghoufi, and P. Malfreyt, J. Chem. Phys. **139**, 024701 (2013).
[31] J. C. Neyt, A. Wender, V. Lachet, A. Ghoufi, and P. Malfreyt, J. Chem. Theory Comput. **10**, 1887 (2014).
[32] J. Benet, L. G. MacDowell, and C. M. na, J. Chem. Eng. Data **55**, 5465 (2010).
[33] R. de Gregorio, J. Benet, N. A. Katcho, F. J. Blas, and L. G. MacDowell, J. Chem. Phys. **136**, 104703 (2012).
[34] F. J. Martínez-Ruiz, F. J. Blas, B. Mendiboure, and A. I. M.-V. Bravo, J. Chem. Phys. **141**, 184701 (2014).
[35] F. J. Martínez-Ruiz, F. J. Blas, L. G. MacDowell, and A. I. M.-V. Bravo, J. Chem. Phys. (2014).
[36] M. P. Allen, *Computer Simulation of Liquids* (Claredon, Oxford, 1987).
[37] D. Frenkel and B. Smit, *Understanding Molecular Simulations* (2nd ed. Academic, San Diego, 2002).
[38] E. M. Blokhius, D. Bedeaux, C. D. Holcomb, and J. A. Zollweg, Mol. Phys. **15**, 665 (1995).
[39] M. Mecke, J. Winkelmann, and J. Fischer, J. Chem. Phys. **107**, 9264 (1997).
[40] M. Mecke, J. Winkelmann, and J. Fischer, J. Chem. Phys. **110**, 1188 (1999).
[41] K. C. Daoulas, V. A. Harmandaris, and V. G. Mavrantzas, Macromolecules **38**, 5780 (2005).
[42] M. Guo and B. C.-Y. Lu, J. Chem. Phys. **106**, 3688 (1997).
[43] J. Janeček, H. Krienke, and G. Schmeer, J. Phys. Chem. B **110**, 6916 (2006).
[44] F. J. Blas, A. I. M.-V. Bravo, J. M. Míguez, M. M. Piñeiro, and L. G. MacDowell, J. Chem. Phys. **137**, 084706 (2012).
[45] M. S. Wertheim, J. Stat. Phys. **35**, 19 (1984).
[46] M. S. Wertheim, J. Stat. Phys. **35**, 35 (1984).
[47] M. S. Wertheim, J. Stat. Phys. **42**, 459 (1986).
[48] M. S. Wertheim, J. Stat. Phys. **42**, 477 (1986).
[49] F. J. Blas and L. F. Vega, Mol. Phys. **92**, 135 (1997).
[50] F. J. Blas and L. F. Vega, Ind. Eng. Chem. Res. **37**, 660 (1998).
[51] A. Harasima, Adv. Chem. Phys. **1**, 203 (1958).
[52] R. Eppenga and D. Frenkel, Mol. Phys. **52**, 1303 (1984).
[53] V. I. Harismiadis, J. Vorholz, and A. Z. Panagiotopoulos, J. Chem. Phys. **105**, 8469 (1996).
[54] F. J. Blas, F. J. Martínez-Ruiz, A. I. M.-V. Bravo, and L. G. MacDowell, J. Chem. Phys. **137**, 024702 (2012).
[55] F. J. Blas and B. Mendiboure, J. Chem. Phys. **138**, 134701 (2013).
[56] F. J. Blas, A. I. M.-V. Bravo, J. A. Fernández, F. J. Martínez-Ruiz, and L. G. MacDowell, J. Chem. Phys. (2014).
[57] J. M. Míguez, M. M. Piñeiro, and F. J. Blas, J. Chem. Phys. **138**, 034707 (2013).
[58] F. Llovell, A. Galindo, G. Jackson, and F. J. Blas, J. Chem. Phys. **133**, 024704 (2010).
[59] R. L. Scott and P. H. van Konynenburg, Discuss. Faraday Soc. **49**, 87 (1970).
[60] P. H. van Konynenburg and R. L. Scott, Phil. Trans. **A298**, 495 (1980).
[61] H. T. Davies and L. E. Scriven, Adv. Chem. Phys. **49**, 357 (1982).

Table 1. Liquid density, ρ^L, vapour density, ρ^V, liquid density of component 1, ρ_1^L, vapour density of component 1, ρ_1^V, liquid density of component 2, ρ_2^L, and vapour density of component 2, ρ_2^V at $T = 1.6$ and different pressures P_N^{vir}, for mixtures of LJ molecules with different dispersive energy parameters, $\epsilon_{22}/\epsilon_{11}$, and a cutoff distance $r_c = 3$ with inhomogeneous LRC. All quantities are expressed in the reduced units defined in Section II. The errors are estimated as explained in the text.

P_N^{vir}	$\rho^{(L)}$	$\rho^{(V)}$	$\rho_1^{(L)}$	$\rho_1^{(V)}$	$\rho_2^{(L)}$	$\rho_2^{(V)}$
			$\epsilon_{22}/\epsilon_{11} = 1.5$			
0.05863(18)	0.6585(2)	0.0463(4)	0.00657(10)	0.00180(4)	0.65194(21)	0.0444(4)
0.07691(22)	0.6430(4)	0.0632(3)	0.0561(3)	0.01667(11)	0.5869(5)	0.04654(21)
0.0961(3)	0.6182(3)	0.0835(8)	0.1045(3)	0.0331(4)	0.5136(6)	0.0504(3)
0.1179(6)	0.5950(4)	0.1124(10	0.1467(2)	0.0538(5)	0.4483(5)	0.0586(5)
0.1361(4)	0.5531(6)	0.1411(17)	0.19249(12)	0.0766(7)	0.3606(5)	0.0644(9)
			$\epsilon_{22}/\epsilon_{11} = 1.75$			
0.0420(13)	0.7349(3)	0.02881(17)	0.03763(20)	0.01176(15)	0.6973(3)	0.01705(13)
0.0731(7)	0.7122(4)	0.0553(4)	0.1088(8)	0.0349(3)	0.6034(12)	0.02032(18)
0.0955(8)	0.6908(3)	0.0758(3)	0.1607(3)	0.05467(23)	0.5301(5)	0.02117(15)
0.1118(8)	0.67272(19)	0.0928(4)	0.1973(3)	0.0689(3)	0.4753(3)	0.0238(3)
0.1315(6)	0.6392(3)	0.1206(8)	0.2509(3)	0.0930(5)	0.3882(5)	0.0276(3)
0.1486(8)	0.6102(4)	0.1473(11)	0.28281(17)	0.1163(8)	0.3274(5)	0.0311(4)
			$\epsilon_{22}/\epsilon_{11} = 2.0$			
0.05126(15)	0.7822(3)	0.03595(16)	0.0679(3)	0.02838(13)	0.7144(4)	0.00757(9)
0.06980(14)	0.7749(3)	0.0491(3)	0.0935(6)	0.0405(3)	0.6814(9)	0.00858(6)
0.0868(12)	0.7638(3)	0.0646(3)	0.1285(7)	0.05562(23)	0.6353(9)	0.00898(8)
0.1069(12)	0.7485(3)	0.0829(4)	0.1733(5)	0.0728(4)	0.5751(7)	0.01011(12)
0.1235(6)	0.7352(3)	0.1040(7)	0.2041(7)	0.0911(6)	0.5311(10)	0.01296(14)
0.1464(15)	0.7083(3)	0.1262(4)	0.2628(10)	0.1121(4)	0.4455(13)	0.01416(13)

Table 2. Normal component of the macroscopic pressure tensor calculated from the virial route $P_N^{\rm vir}$, normal and tangential components of the macroscopic pressure tensor calculated from VP, P_N and P_T, surface tension calculated from integration given by Eq. (7), γ^{vir}, from VP, γ, and from TA, γ_{TA}, and $10-90$ interfacial thickness, t, at $T = 1.6$ and different pressure for mixtures of LJ molecules with different dispersive energy parameters, $\epsilon_{22}/\epsilon_{11}$, and a cutoff distance $r_c = 3$ with inhomogeneous LRC. All quantities are expressed in the reduced units defined in Section II. The errors are estimated as explained in the text. Uncertainties of surface tension calculated from the virial route, γ^{vir}, are error estimates corresponding to the numerical calculation of the integral given by Eq. (7).

P_N^{vir}	P_N^*	P_T^*	γ^{vir}	$\gamma*$	γ_{TA}	t
		$\epsilon_{22}/\epsilon_{11} = 1.5$				
0.05863(18)	0.0586(7)	0.0473(6)	0.565(5)	0.56(4)	0.559(5)	4.090(5)
0.07691(22)	0.0801(6)	0.0701(6)	0.438(3)	0.44(3)	0.438(4)	4.63(4)
0.0961(3)	0.0947(7)	0.0869(6)	0.333(3)	0.32(3)	0.320(4)	5.49(6)
0.1179(6)	0.1148(4)	0.1093(4)	0.258(3)	0.24(2)	0.251(3)	6.46(15)
0.1361(4)	0.1316(5)	0.1283(5)	0.166(2)	0.15(3)	0.153(4)	7.97(17)
		$\epsilon_{22}/\epsilon_{11} = 1.75$				
0.0420(13)	0.0423(10)	0.0178(10)	1.025(4)	1.03(6)	1.027(6)	3.069(10)
0.0731(7)	0.0735(7)	0.0572(7)	0.730(4)	0.73(4)	0.742(6)	3.91(11)
0.0955(8)	0.0944(8)	0.0803(7)	0.554(3)	0.55(4)	0.552(6)	4.49(7)
0.1118(8)	0.1097(8)	0.0998(7)	0.431(3)	0.42(4)	0.424(4)	5.234(5)
0.1315(6)	0.1308(8)	0.1242(8)	0.294(3)	0.28(4)	0.280(3)	6.455(11)
0.1486(8)	0.1478(8)	0.1432(8)	0.204(2)	0.19(5)	0.190(4)	8.111(19)
		$\epsilon_{22}/\epsilon_{11} = 2.0$				
0.05126(15)	0.0506(7)	0.0209(6)	1.312(5)	1.32(4)	1.321(9)	2.99(8)
0.06980(14)	0.0666(7)	0.0418(7)	1.085(4)	1.09(4)	1.095(6)	3.46(8)
0.0868(12)	0.0838(7)	0.0618(7)	0.959(4)	0.96(4)	0.967(6)	3.761(18)
0.1069(12)	0.1048(8)	0.0865(7)	0.753(3)	0.75(4)	0.748(8)	4.323(5)
0.1235(6)	0.1200(7)	0.1070(7)	0.605(3)	0.60(4)	0.594(9)	5.181(16)
0.1464(15)	0.1465(9)	0.1365(9)	0.422(2)	0.41(5)	0.415(7)	6.362(4)

(a)

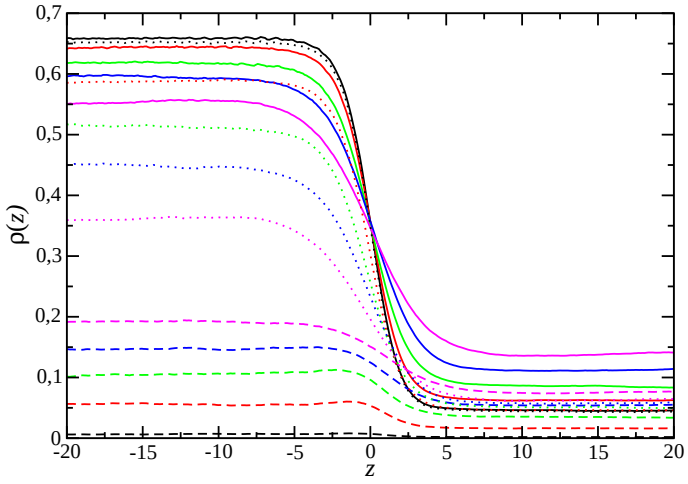

(b)

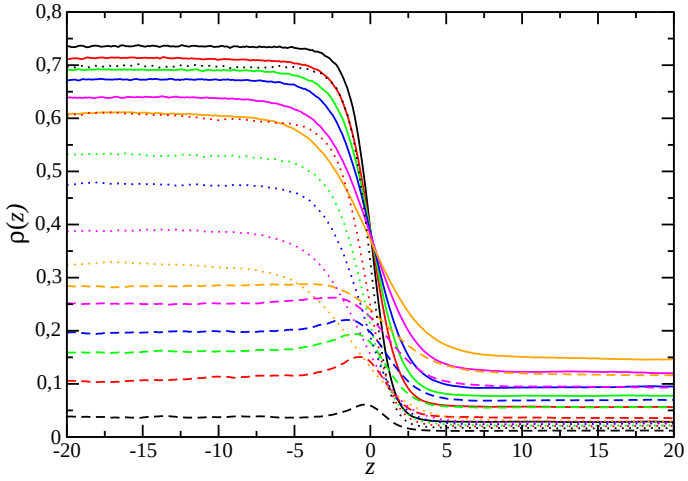

(c)

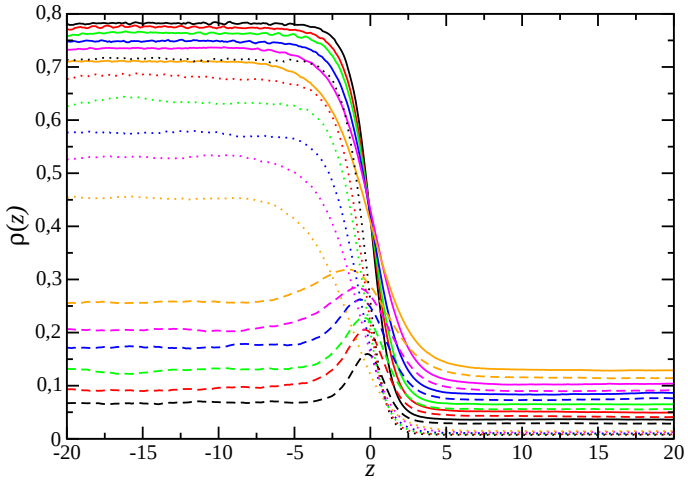

Figure 1. Simulated equilibrium total density profiles (continuous curve), density profiles of component 1 (dotted curve) and density profiles of component 2 (dashed curve) across the vapour-liquid interface of mixtures of spherical LJ molecules with the same molecular size and dispersive energy ratio $\epsilon_{22}/\epsilon_{11} = 1.50$ (a), 1.75 (b), and 2.0 (c). Pressure of system is equal to, from top to bottom in the liquid phase, $P^* = 0.06$ (black), 0.08 (red), 0.10 (green), 0.12 (blue), 0.14 (magenta), and 0.16 (orange).

(a)

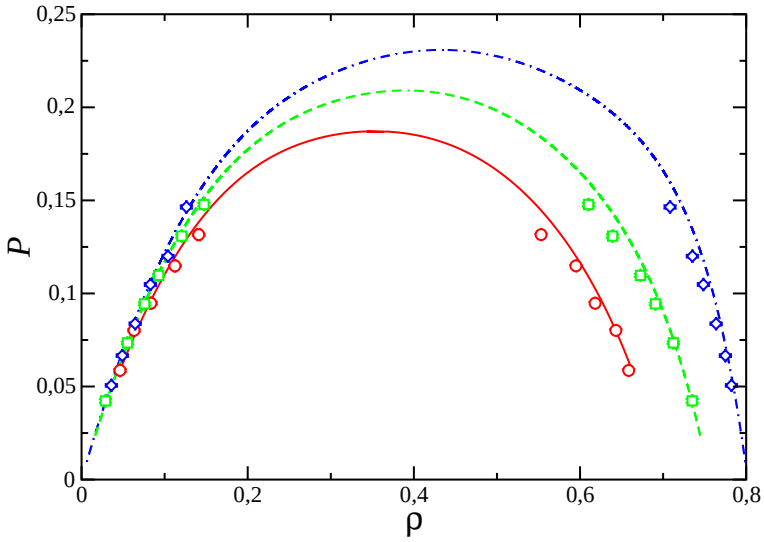

(b)

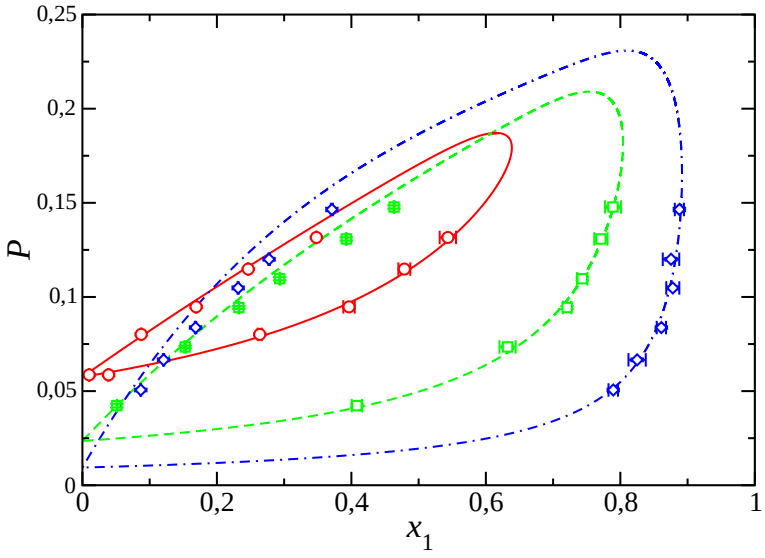

Figure 2. Pressure-density (a) and pressure-composition (b) slices of the phase diagram of mixtures of spherical LJ molecules with the same molecular size and dispersive energy ratio $\epsilon_{22}/\epsilon_{11} = 1.5$ (red circles and continuous curves), 1.75 (green squares and dashed curves), and 2.0 (blue diamonds and dash-dotted curves). Symbols correspond to simulation data obtained in this work and curves are the predictions obtained from the Soft-SAFT equation of state.

(a)

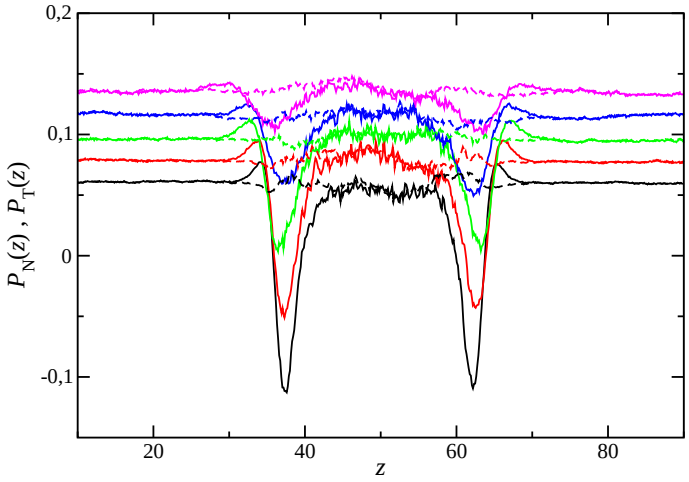

(b)

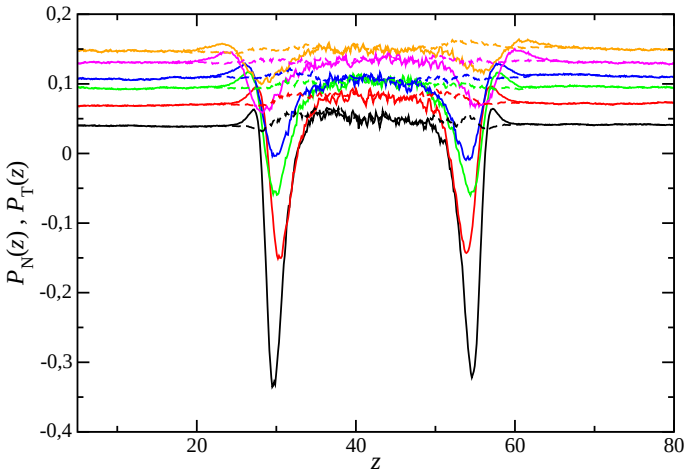

(c)

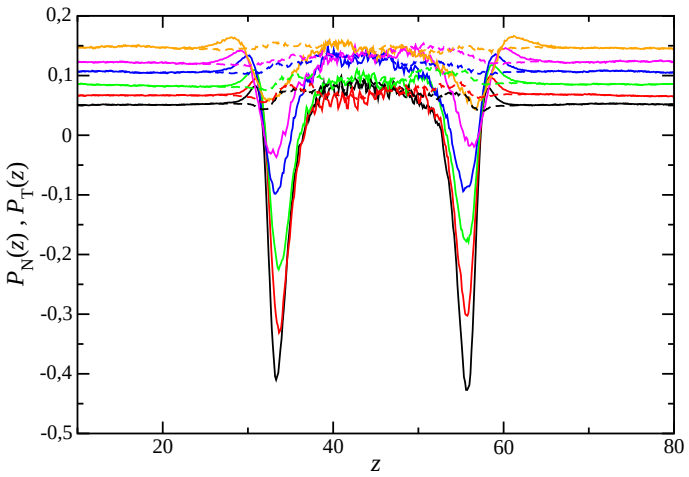

Figure 3. Normal $P_N(z)$ and tangential $P_T(z)$ microscopic components of pressure tensor profiles across the two vapor-liquid interface at $T = 1.6$ and $P = 0.06$ (black curves), 0.08 (red curves), 0.10 (green curves), 0.12 (blue curves), 0.14 (magenta curves), and 0.16 (orange curves) of binary mixtures of spherical LJ molecules with the same molecular size and different dispersive energy ratios $\epsilon_{22}/\epsilon_{11} = 1.5$ (a), 1.75 (b), and 2.0 (c). Continuous and dashed curves correspond to tangential and normal microscopic components of the pressure tensor, respectively.

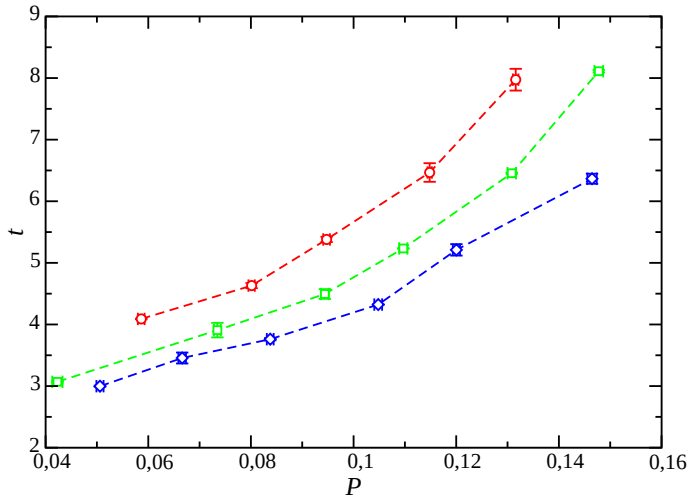

Figure 4. The $10-90$ interfacial thickness as a function of the pressure for mixtures of spherical LJ molecules with the same molecular size and dispersive energy ratio $\epsilon_{22}/\epsilon_{11} = 1.5$ (red circles), 1.75 (green squares), and 2.0 (blue diamonds). Symbols correspond to simulation data obtained in this work and curves are included as a guide to eyes.

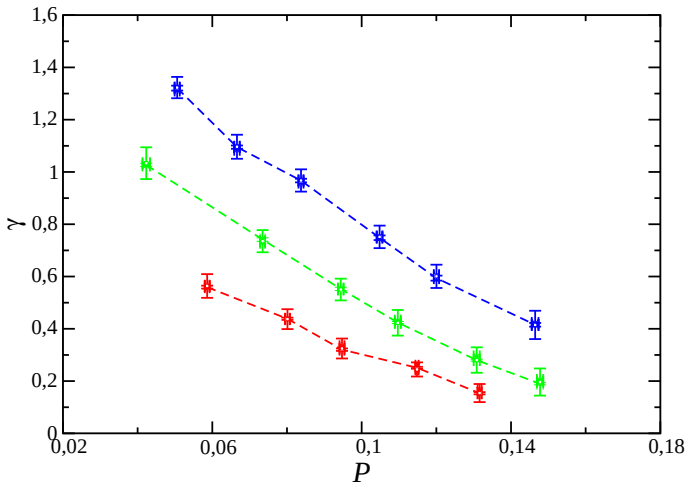

Figure 5. Surface tension as a function of pressure for mixtures of spherical LJ molecules with the same molecular size and dispersive energy ratio $\epsilon_{22}/\epsilon_{11} = 1.5$ (red), 1.75 (green), and 2.0 (blue). Different symbols represent the surface tension obtained from MC NVT simulations for spherical molecules using the mechanical route of Irving and Kirkwood [8] (open circles), the VP method of de Miguel and Jackson [9] (open squares), and the TA technique [3] (crosses). The curves are included as a guide to eyes.